Carbazole and Simplified Derivatives: Novel Tools toward *β*-Adrenergic Receptors Targeting

Fedora Grande [1,†], Anna De Bartolo [2,†], Maria Antonietta Occhiuzzi [1], Anna Caruso [1,*], Carmine Rocca [2], Teresa Pasqua [3], Alessia Carocci [4], Vittoria Rago [1], Tommaso Angelone [2] and Maria Stefania Sinicropi [1]

1   Department of Pharmacy, Health and Nutritional Sciences, University of Calabria, 87036 Arcavacata di Rende, Italy; fedora.grande@unical.it (F.G.); mariaantonietta.occhiuzzi@unical.it (M.A.O.); vittoria.rago@unical.it (V.R.); s.sinicropi@unical.it (M.S.S.)
2   Laboratory of Cellular and Molecular Cardiovascular Pathophysiology, Department of Biology, E and E.S. (DiBEST), University of Calabria, 87036 Arcavacata di Rende, Italy; anna.debartolo@unical.it (A.D.B.); carmine.rocca@unical.it (C.R.); tommaso.angelone@unical.it (T.A.)
3   Department of Health Science, University of Catanzaro Magna Graecia, 88100 Catanzaro, Italy; teresa.pasqua@unicz.it
4   Department of Pharmacy-Pharmaceutical Sciences, University of Bari Aldo Moro, 70126 Bari, Italy; alessia.carocci@uniba.it
*   Correspondence: anna.caruso@unical.it; Tel.: +39-0984-493019
†   These authors equally contributed to this work.

Abstract: *β*-Adrenergic receptors (*β*-ARs) are G protein-coupled receptors involved in important physiological and pathological processes related to blood pressure and cardiac activity. The inhibition of cardiac *β*1-ARs could be beneficial in myocardial hypertrophy, ischemia and failure. Several carbazole-based compounds have been described as promising *β*-blockers. Herein, we investigate the capability of a carbazole derivative and three simplified indole analogs to interact with the active binding site of *β*1-AR by molecular docking studies. In the light of the obtained results, our compounds were tested by biological assays in H9c2 cardiomyocytes exposed to isoproterenol (ISO) to confirm their potential as *β*1-blockers agents, and two of them (**8** and **10**) showed interesting and promising properties. In particular, these compounds were effective against ISO-dependent in vitro cardiac hypertrophy, even at concentrations lower than the known *β*-AR antagonist propranolol. Overall, the data suggest that the indole derivatives 8 and 10 could act as potent *β*1-blockers and, active at low doses, could elicit limited side effects.

Keywords: *β*-blockers; carbazole; indole; molecular docking; H9c2 cells; cardiac hypertrophy

1. Introduction

Over the last decades, *β*-blockers (i.e., antagonists of *β*-adrenergic receptors, *β*-ARs) have emerged as crucial therapeutic agents in the first-line treatment of acute and chronic diseases, particularly in the field of cardiovascular pathologies.

β-ARs are G protein-coupled receptors used by endogenous catecholamines, especially noradrenaline and adrenaline [1], to modulate important physiological processes, such as blood pressure and cardiac activity [2]. Starting from their discovery, which gained Sir Henry H. Dale the Nobel Prize in 1936 [3], *β*-ARs have become crucial targets in the therapy of cardiovascular diseases [4]. Indeed, it is widely accepted that a deep relationship between *β*-ARs and the cardiovascular role of the sympathetic nervous system (SNS) exists. The history of *β*-blockers has been heavily influenced by the finding of three different *β*-ARs subtypes that paved the way for the design and the development of selective agonists and antagonists with specific therapeutic goals. It is known that *β*1-ARs are mainly expressed in the heart, *β*2-ARs in the smooth muscle of vasculature and airways and *β*3-ARs in the adipose tissue [2]. Cardiovascular therapies were deeply influenced and revolutionized when propranolol was introduced for the first time in the clinic for its ability to reduce

myocardial oxygen demand under angina episodes [5,6]. Since then, three generations of β-ARs antagonists have been developed, namely nonselective, β1-cardioselective and β1-blockers with vasodilation activity [2].

In the heart, β1-ARs, β2-ARs and β3-ARs are all expressed and modulate cardiac performance by activating key intracellular pathways [7]. The homeostatic role of β-ARs in cardiac physiology is significantly highlighted by their strong phylogenetic conservation among species [8–10].

However, the effects on the myocardium are predominantly mediated by β1-ARs and β2-ARs, since in the healthy heart they are more expressed with respect to β3-ARs [4,11].

Stress stimuli, such as increased activity of the SNS, cause augmented plasma catecholamine levels by an adaptive physiological response. However, if stress and high catecholamine levels become chronic, the overactivation of β-ARs may result in an aberrant signaling network that leads to cardiac remodeling, fibrosis, arrhythmia, ventricular hypertrophy and heart failure [4,11]. In this perspective, the role of β-blockers to counteract detrimental effects of chronic stress assumes a critical significance.

In terms of pharmacological classification, all β-blockers share a common feature that consists in their affinity/ability to bind β-ARs without evoking physiological effects. They are generally classified as competitive antagonists, so their effect can be overcome by increasing agonist concentration [12]. In particular, the blockade of cardiac β1-ARs is beneficial in myocardial hypertrophy, ischemia and failure, reducing both oxygen demand and renin production at a systemic level [13].

Much experimental and clinical evidence demonstrate that SNS overactivation and the resulting increase in catecholamine plasma levels is involved in the development of cardiac hypertrophy. In particular, the stimulation of β1-ARs, that in turn increases intracellular levels of cyclic-AMP and consequently of Ca^{2+}, may account for the activation of the cardiac hypertrophic pathway [14,15]. In this view, the possibility to design and develop even more selective β1-ARs blockers still represents an important goal for cardiovascular translational research and an open field to be investigated [16–20].

In the literature, several compounds endowed with a carbazole structure or with a simplified carbazole moiety are reported as β-blockers. In particular, carvedilol has been widely studied as a third-generation β-blocker [21], carazolol as a high affinity inverse agonist of the β-adrenergic receptor [22], pindolol as a nonselective β-blocker, which is used in the treatment of hypertension [23], and bucindolol (Figure 1) as a nonselective β-blocker with weak α-blocking properties and intrinsic sympathomimetic activity [24].
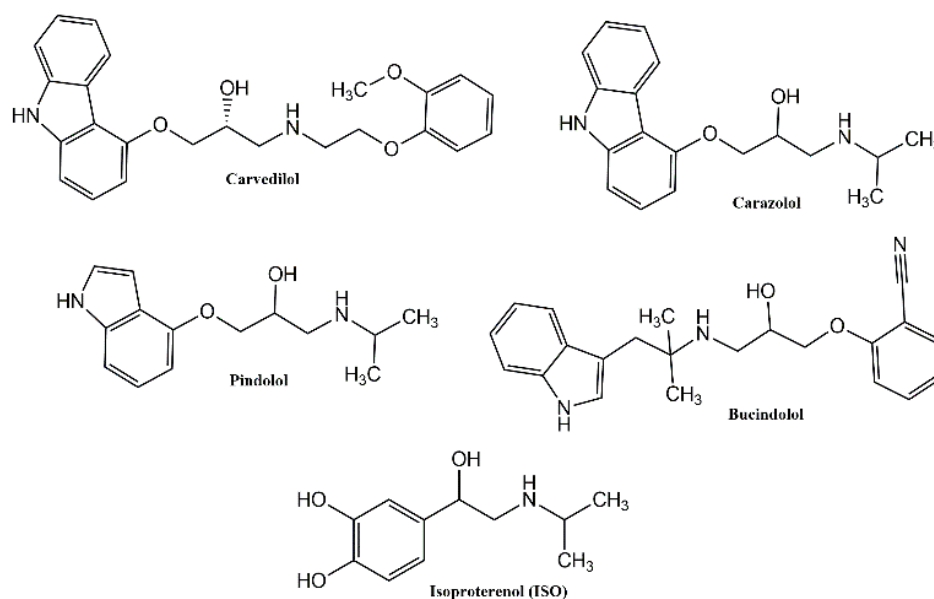

Figure 1. Representative structures of known β-blockers.

Based on this knowledge, the present study was undertaken to investigate the molecular interactions of a carbazole derivative, 4, and its three simplified analogs (7, 8, 10) with the active binding site of β1-AR. Considering the promising results obtained in silico, the in vitro bioactivity of these compounds was evaluated. In particular, we used the β-AR agonist isoproterenol (ISO, Figure 1) as a suitable hypertrophy-causing drug in H9c2 cells. This is a cell line widely used as model of cardiomyocytes for its biochemical, morphological and electrical/hormonal signaling properties [15]. Interesting results have been obtained for compounds **8** and **10** (Figure 2) making them novel tools against ISO-dependent in vitro cardiac hypertrophy.
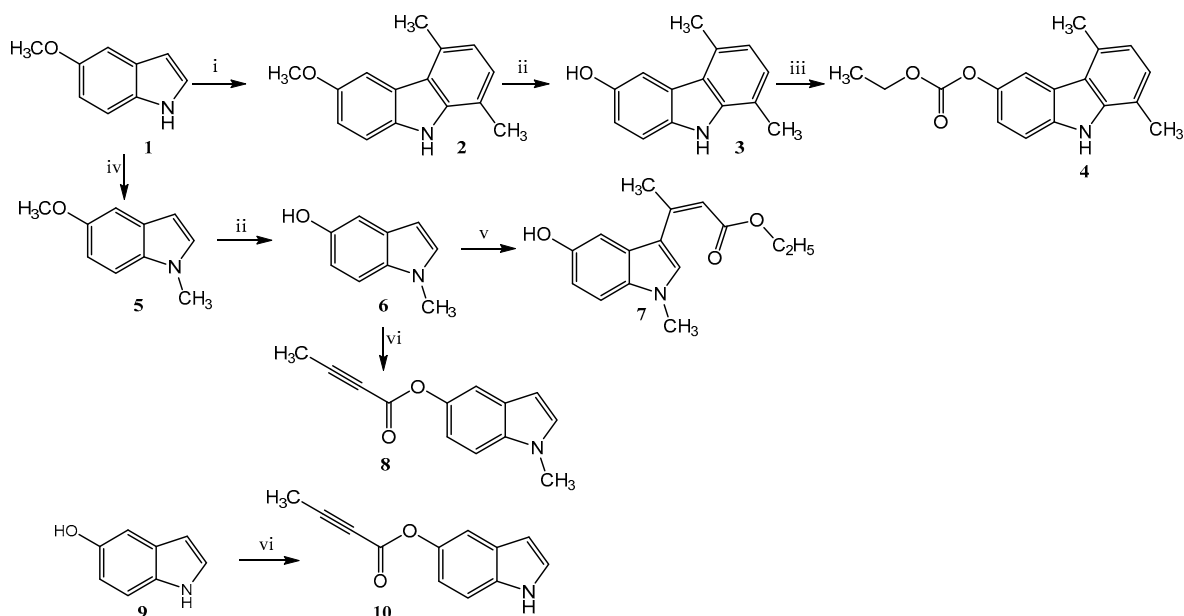
Figure 2. Reagents: (i) acetonylacetone, *p*-TSA, ethanol, reflux, 6 h; (ii) anhydrous pyridine hydrochloride, reflux, 2 h; (iii) ethyl chloroformate, NaOH solution 1N, acetone, reflux, 4 h; (iv) NaH, CH$_3$I, DME, 25 °C; (v) ethyl acetoacetate (1 mol), indium (III) chloride, reflux, 2 h; (vi) but-2-ynoic acid, DCC, DMAP, CH$_2$Cl$_2$/DMF (10:1), r.t. 2 h.

2. Materials and Methods

2.1. Chemistry

Commercial reagents were purchased from Aldrich, Acros Organics and Alfa Aesar and used without additional purification. Melting points were determined on a Kofler melting point apparatus. IR spectra were taken with a Perkin Elmer BX FT-IR. Mass spectra were taken on a JEOL JMS GCMate spectrometer at an ionizing potential of 70 eV (EI) or were performed using a spectrometer LC-MS Waters alliance 2695 (ESI+) or ESI mass spectrometer Finnigan LCQ Advantage max. ^{1}H-NMR (400 MHz) and ^{13}C-NMR (100 MHz) were recorded on a JEOL Lambda 400 Spectrometer. Chemical shifts were expressed in parts per million downfield from tetramethylsilane as an internal standard. The 2, 3, 5, 6 intermediates and the final product 4, 7, 8, 10 were prepared as described in the literature [25–30].

2.1.1. 1,4-Dimethyl-6-methoxy-carbazole (**2**)

A mixture of 5-methoxyindole (**1**) (25.0 mmol), acetonylacetone (31.0 mmol) and *p*-TSA (20.0 mmol), in ethanol (60 mL) was heated to reflux for 6 h and then concentrated in vacuo. The crude product was purified by chromatography on silica gel using ethyl acetate:n-hexane, 2:8 as eluent. White solid, yield 57%, mp 150 °C. IR (KBr) (cm^{-1}): 3406, 2959, 1481, 1210, 1045, 812, 545. ^{1}H NMR (DMSO-d$_6$): δ 11.01 (br, 1H, NH); 7.64 (s, 1H, Ar); 7.48 (d, J = 8.56 Hz, 1H, Ar); 7.09 (d, J = 8.28 Hz, 2H, Ar); 6.85 (d, J = 7.08 Hz, 1H, Ar); 3.90 (s, 3H, OCH$_3$); 2.69 (s, 3H, CH$_3$); 2.62 (s, 3H, CH$_3$). ^{13}C NMR (DMSO-d$_6$): δ 152.5; 139.5;

134.4; 129.3; 125.3, 123.4; 120.1; 119.2; 117.1; 111.1; 105.0; 55.3; 19.9; 16.5. MS (ESI+): 226 (M^+ +1), 224 (M^+ −1).

2.1.2. 1,4-Dimethyl-6-hydroxy-carbazole (3)

A mixture of 1,4-dimethyl-6-methoxy-carbazole (**2**) and anhydrous pyridine hydrochloride (1:16) was heated to reflux for 2 h. The reaction mixture was left to cool to room temperature, then ice water was added. The product was extracted with Et_2O. The organic layer was washed with a solution of HCl (2N), dried over $MgSO_4$ and concentrated in vacuum. White solid, yield 75%, mp 174 °C. IR (KBr) (cm^{-1}): 3517, 3415, 1461, 1165, 847, 809, 543. ^1H NMR (DMSO-d_6): δ 10.88 (s, 1H, NH); 9.12 (bs, 1H, OH); 7.53 (s, 1H, Ar); 7.40 (d, J = 8.56 Hz, 1H, Ar); 7.08 (d, J = 7.36 Hz, 1H, Ar); 6.95 (d, J = 8.56 Hz, 1H, Ar); 6.83 (d, J = 7.36 Hz, 1H, Ar); 2.61 (s, 3H, CH_3); 2.50 (s, 3H, CH_3). ^{13}C NMR (DMSO-d_6): δ 150.2; 139.7; 133.8; 129.4; 125.4, 123.9; 120.3; 119.2; 117.2; 114.0; 111.1; 107.0; 20.1; 16.7. MS (ESI+): 212 (M^+ +1).

2.1.3. 5,8-Dimethyl-9H-carbazol-3-yl Ethyl Carbonate (4)

A mixture of NaOH solution 1N (50 mL) and acetone (50 mL) was added 1,4-dimethyl-6-hydroxy-carbazole (**3**) (31.0 mmol) and ethyl chloroformate (37.0 mmol). The reaction mixture was heated to reflux for 4 h and then was extracted with Et_2O. The organic layer was washed with a solution of NaOH (0.5%), dried over $MgSO_4$ and concentrated in vacuum. White solid, yield 91%, mp 130 °C. IR (KBr) (cm^{-1}): 3396, 1744, 1462, 1253, 1181, 1002, 811, 780, 552. ^1H NMR (DMSO-d_6): δ 11.36 (s, 1H, NH); 7.94 (s, 1H, Ar); 7.58 (d, 1H, J = 8.56 Hz, Ar); 7.29 (dd, 1H, J_1 = 1.72 Hz, J_2 = 8.56 Hz, Ar); 7.16 (d, 1H, J = 7.32 Hz, Ar); 6.91 (d, 1H, J = 7.08 Hz, Ar); 4.35–4.28 (q, 2H, CH_2CH_3); 2.78 (s, 3H, CH_3); 2.57 (s, 3H, CH_3); 1.40–1.32 (t, 3H, CH_2CH_3). ^{13}C NMR (DMSO-d_6): δ 153.9; 143.5; 139.8; 137.5; 129.7; 126.2, 123.1; 120.2; 120.0; 118.3; 117.6; 114.1; 111.0; 64.3; 20.0; 16.6; 14.0. MS (ESI+): 284 (M^+ +1). ESI m/z calcd for $C_{17}H_{18}NO_3$: 284.13; found: 284.10.

2.1.4. 5-Methoxy-1-methylindole (5)

To a stirred cold solution (0 °C) of 5-methoxyindole (**1**) (6.80 mmol) in dry DMF (30 mL), was added NaH 60% oil dispersion (10.20 mmol). After 10 min stirring at this temperature, iodomethane (20.40 mmol) was added and the mixture was further stirred at 25 °C for 1 h. Water (100 mL) was then added to the reaction mixture and the solid product obtained was filtered, washed with water and dried. White solid, yield 92%, mp 114 °C. IR (KBr) (cm^{-1}): 2922, 1621, 1496, 1242, 1151, 1025, 802, 725. ^1H-NMR (DMSO-d_6) δ 7.30 (d, 1H, J = 8.80 Hz, Ar); 7.23 (d, 1H, J = 2.90 Hz, Ar); 7.04–7.01 (m, 1H, Ar); 6.76 (dd, 1H, J = 1.90, 8.80 Hz, Ar); 6.30 (d, 1H, J = 2.90 Hz Ar); 3.72 (s, 6H, NCH_3 and OCH_3). ^{13}C NMR (DMSO-d_6): δ 154.0; 130.6; 129.0; 128.4; 112.3; 111.9; 111.6; 101.1; 56.0; 32.9. MS (ESI+): 162 (M^+ +1).

2.1.5. 5-Hydroxy-1-methylindole (6)

A mixture of 5-methoxy-1-methylindole (**5**) and anhydrous pyridine hydrochloride (1:16) was heated to reflux for 2 h. The reaction mixture was left to cool to 25 °C, then ice water was added. The product was extracted with Et_2O. The organic layer was washed with a solution of HCl (2N), dried over Na_2SO_4 and concentrated in vacuum. Yellow solid, yield 60%, mp 156 °C, IR (KBr) (cm^{-1}): 3177, 2924, 1621, 1489, 1234, 1145, 949, 795, 719. ^1H-NMR (DMSO-d_6) δ 8.67 (s, 1H, OH); 7.19 (s, 1H, Ar); 7.17–7.15 (m, 1H, Ar); 6.81 (d, 1H, J = 3.00 Hz, Ar); 6.62 (dd, 1H, J = 1.90, 8.80 Hz, Ar); 6.18 (d, 1H, J = 2.90 Hz, Ar); 3.04 (s, 3H, NCH_3). ^{13}C NMR (DMSO-d_6): δ 152.5; 130.1; 129.8; 128.7; 116.3; 110.1; 101.6; 100.1; 33.9. MS (ESI+): 148 (M^+ +1).

2.1.6. Ethyl 3-(5-hydroxy-1-methyl-1H-indol-3-yl)but-2-enoate (7)

To a mixture of 5-hydroxy-1-methyl-1*H*-indole (**6**) and ethyl acetoacetate (1 mol), indium(III) chloride (10 mol%) was added under nitrogen. The reaction mixture was

heated under reflux for 2 h, and then it was left to cool to 25 °C. Ice water was added and then the reaction mixture was extracted by ethyl acetate. The organic layer was collected and washed with brine, dried over Na_2SO_4 and concentrated in vacuum. The solid residue was washed with Et_2O. Pink solid, yield 58%, mp 200 °C. IR (KBr) (cm^{-1}): 3400, 2931, 1705, 1488, 1373, 1329, 1201, 1083, 1016, 851, 788. ^{1}H NMR (DMSO- d$_6$) δ 8.32 (s, 1H, Ar); 7.08–7.06 (m, 2H, Ar, OH); 6.52–6.49 (m, 2H, Ar); 6.45 (s, 1H, C=CH); 3.78–3.74 (q, 2H, CH$_2$); 3.67 (s, 3H, NCH$_3$); 1.83 (s, 3H, C-CH$_3$); 0.82–0.78 (t, 3H, CH$_3$). ^{13}C NMR (DMSO-d$_6$): δ 200.4; 153.3; 152.5; 132.1; 129.4; 128.6; 125.1; 116.9; 109.1; 108.7; 103.6; 34.1; 33.9; 20.5; 8.7. MS (EI) *m/z*: 259 (M$^+$, 1). ESI *m/z* calcd for $C_{15}H_{18}NO_3$: 260.13; found: 260.10.

2.1.7. 1-Methyl-1H-indol-5-yl-but-2-ynoate (**8**)

But-2-ynoic acid (1.1 eq), DCC (1 eq) and DMAP (cat) were added to a solution of 5-hydroxy-1-methyl-1H-indole (**6**) in a mixture of CH_2Cl_2 and DMF (10:1). The reaction mixture was stirred at 25 °C for 2 h and then concentrated in vacuum. The solid residue was suspended in ethyl acetate, filtered and the filtrate was washed with brine. The organic layer was dried over anhydrous Na_2SO_4 and evaporated under reduced pressure. The solid residue was purified by silica gel chromatography using ethyl acetate:n-hexane, 2:8 as an eluent.

White solid, yield 64%, mp 90 °C; IR (KBr) (cm^{-1}): 3402, 2233, 1711, 1625, 1487, 1246, 1217, 1123, 1033, 882. ^{1}H NMR (CDCl$_3$) δ 7.28 (s, 1H, Ar); 7.23–7.19 (t, 1H, Ar); 7.01 (d, 1H, J = 3.00 Hz, Ar); 6.98 (dd, 1H, J = 2.00, 8.80 Hz, Ar); 6.46 (d, 1H, J = 3.00 Hz, Ar); 3.70 (s, 3H, NCH$_3$); 2.06 (s, 3H, C-CH$_3$). ^{13}C NMR (CDCl$_3$): δ 149.4; 143.3; 133.5; 128.9; 128.4; 119.6; 109.4, 108.7; 100.1; 86.9; 76.1; 34.7; 3.6. MS (ESI+): 214 (M$^+$ +1). ESI *m/z* calcd for $C_{13}H_{12}NO_2$: 214.09; found: 214.03.

2.1.8. Indol-5-yl-but-2-ynoate (**10**)

But-2-ynoic acid (1.1 eq), DCC (1 eq) and DMAP (cat) were added to a solution of 5-hydroxyindole (**9**) in a mixture of CH_2Cl_2 and DMF (10:1). The reaction mixture was stirred at room temperature for 2 h, and then concentrated in vacuum. The solid residue was suspended in ethyl acetate, filtered and the filtrate was washed with brine. The organic layer was dried over anhydrous Na_2SO_4 and evaporated under reduced pressure. The solid residue was purified by silica gel chromatography using ethyl acetate:petroleum ether, 2:8 as eluent.

White solid, yield 62%, mp 108 °C. IR (KBr) (cm^{-1}): 3410, 2237, 1705, 1480, 1261, 1121, 884. ^{1}H NMR (CDCl$_3$) δ 8.25 (bs, 1H, NH); 7.40 (s, 1H, Ar); 7.20–7.23 (m, 1H, Ar); 7.03–7.01 (m, 1H, Ar); 6.95 (dd, 1H, J = 1.90, 8.80 Hz, Ar); 6.60–6.50 (m, 1H, Ar); 2.10 (s, 3H, C-CH$_3$). ^{13}C NMR (CDCl$_3$): δ 149.1; 140.3; 134.5; 128.7; 124.4; 119.6; 111.4; 109.7; 102.1; 86.9; 75.1; 3.4. GC-MS *m/z*: 199 [M$^+$]. ESI *m/z* calcd for $C_{12}H_9NO_2$: 199.06; found: 199.15.

2.2. Molecular Docking

Molecular docking of compounds 4, 7, 8 and 10 was carried out on the crystallographic structure of human $β1$-AR (PDB code 7BVQ). The binding pathway determines norepinephrine selectivity for the human beta 1 AR over beta 2 AR [22]. The molecular structures of the ligands were built by using the modeling software Avogadro [31]. Preliminary conversion of the structures from the PDB format was carried out by using the graphical interface AutoDock Tools 1.5.6 [32]. During the conversion, polar hydrogens were added for the crystallographic enzyme and apolar hydrogens of all compounds were merged to the carbon atom they were attached to. Docking calculations were performed by using AutoDock Vina1.1.2 [33] exploring the search volume that included the protein structure, and by performing a score-only assessment without any search in the case of redocking of the crystallographic ligand in its known binding mode. In the former case a very high exhaustiveness search was used, 8 time larger than the default value [34,35], facilitated by the relatively small number of active torsions around bond dihedral angles necessary to give full flexibility to the ligands (four degrees of freedom for 4 and three for

7, 8 and 10). The binding modes of the ligands were analyzed through visual inspection, and interactions energies and distances were quantified by using Molecular Operating Environment (MOE) 2018.01 (Chemical Computing Group ULC, Montreal, QC, Canada). The Molecular Graphics System PyMOL was used to visualize protein structure and the bonded ligands (PyMOL Molecular Graphics System, Version 1.2r3pre, Schrödinger, LLC., IN, New York, NY, USA)

2.3. Cell Culture

H9c2 cells (ATCC, CRL-1446, Manassas, VA, USA) and rat embryonic cardiomyocytes were cultured in DMEM/F-12 (Gibco, Thermo Fisher Scientific, Waltham, MA, USA) supplemented with 10% fetal bovine serum (FBS, Gibco) and 1% penicillin/streptomycin (Thermo Fisher Scientific) in a humidified incubator with 5% CO_2 at 37 °C. After reaching 80% confluence in 100-mm dishes, cells were detached by using 0.25% Trypsin-EDTA (1X) (Gibco) at 1:2 ratio following the manufacturer's instructions (ATCC). Cells were seeded and incubated for two days at 37 °C, 95% O_2 and 5% CO_2 before treatments.

2.4. 3-(4,5-Dimethylthiazol-)2,5-diphenyl Tetrazolium Bromide (MTT) Assay

H9c2 cell viability was evaluated by 3-(4,5-dimethylthiazol-2-yl)-2,5-diphenyltetrazolium bromide (MTT) assay, as previously described [36,37] Cells were seeded at a density of 5×10^3 cells/well in 96-well plate and then treated with compound 8 or compound 10 (1 nM–100 nM) for 24 h. Control cells were treated with vehicle. At the end of the treatments, the cell culture medium was replaced with 100 μL of 2 mg/mL MTT solution (Sigma Aldrich) and cells were incubated for 4 h at 37 °C, 5% CO_2. After MTT incubation, the solution was removed and the formazan crystals were solubilized in DMSO for 30 min. The absorbance was recorded using a Multiskan EX Microplate Reader Lab (Thermo Fisher Scientific) at 570 nm. The means of absorbance values of six wells in each experimental group were expressed as the percentage of cell viability. Cell viabilities were calculated as percentage of cell survival relative to the control [38,39].

2.5. Morphological Analysis of H9c2 Cells

The morphological alterations in H9c2 cells were evaluated by May-Grunwald Giemsa staining as previously described [36]. Cells were seeded in 60-mm dishes and exposed to the following treatments: control (vehicle), ISO (100 μM) alone, compound 8 (10, 25, 50, 75 and 100 nM), ISO + 8 (10, 25, 50, 75 and 100 nM), compound 10 (10, 25, 50, 75 and 100 nM), ISO + 10 (10, 25, 50, 75 and 100 nM) for 24 h. As positive control, the β-AR antagonist propranolol (PROP) (1 μM) was used alone or in cotreatment with ISO for 24 h [40]. After staining, cells were displayed by Olympus BX41 microscope and the images were taken with CSV1.14 software, using a CAM XC-30 for image acquisition. The cell surface area measurement was analyzed by using Image J 1.6 (NIH). Data were expressed as percentage of relative increase in cell surface area.

2.6. Statistical Analysis

Data, expressed as mean ± SEM, were analyzed by one-way ANOVA and Dunnett's Multiple Comparison Test (for post ANOVA comparisons) or nonparametric Newman-Keuls Multiple Comparison Test (for post-ANOVA comparisons) when appropriate. Values of * $p \leq 0.05$, ** $p \leq 0.01$, *** $p \leq 0.001$ were considered statistically significant versus the control group, while values of # $p \leq 0.05$, ## $p \leq 0.01$, ### $p \leq 0.001$ were considered statistically significant versus the ISO group. The statistical analysis was carried out using Graphpad Prism 5 (GraphPad Software, La Jolla, CA, USA).

3. Results and Discussion

3.1. Chemistry

Compound 4, endowed with a carbazole scaffold, and its simplified derivatives 7, 8, 10 were synthesized following chemical procedures previously reported (Figure 2) [25–28,41].

In particular, the carbazole 4 was prepared by a three-step synthesis. The starting material 5-methoxyndole 1, was used to obtain the 1,4-dimethyl-6-methoxy-carbazole (**2**) by Cranwell and Saxton reaction [26,42]. The demethylation of derivative **2**, by heating under reflux in anhydrous pyridine hydrochloride, gave the 1,4-dimethyl-6-hydroxy-carbazole (**3**) [27]. In the last step, the derivative but-2-ynoic acid (1.1 eq), DCC (1 eq) and DMAP (cat) were added. was prepared by reaction of 3 with ethyl chloroformate under standard conditions [43,44]. Ethyl 3-(5-hydroxy-1-metyl-1*H*-indol-3-yl)but-2-enoate (**7**) was instead prepared by von Pechmann reaction [41] using 5-hydroxy-1-methylindole (**6**) and Indium(III) chloride as catalyst. This latter, 6, was obtained starting from 5 by selective demethylation of the methoxyl group, in a similar manner as above reported for the preparation of derivative 3 [45]. 5-Methoxy-1-methylindole (**5**) was prepared using 1 as starting material 1 by *N*-methylation with NaH and methyl iodide. Finally,1-methyl-1*H*-indol-5-yl-but-2-ynoate (**8**) was synthesized by esterification of 6 with but-2-ynoic acid in a mixture of CH_2Cl_2, DMF, DCC and DMAP [41]. The same synthetic procedure was used for the preparation of indol-5-yl-but-2-ynoate (**10**) starting from 5-hydroxy-indole (**9**) [41].

3.2. Molecular Docking

In order to investigate the molecular interactions between compounds 4, 7, 8 and 10 and the active binding site of *β*1-adrenergic receptor, molecular docking studies were performed on a crystallographic structure of the target protein obtained from the Protein Data Bank (PDB code 7BVQ) [22]. In this structure the receptor is complexed with carazolol, a previously identified inverse agonist endowed with a carbazole based chemical structure [22]. In the PDB is reported another interesting crystallographic structure of *β*1 receptor (PDB code 7JJO), very recently deposited, in which the protein is complexed with ISO, a known *β*1-adrenergic receptor ligand. Even though this structure presents a more complete aminoacidic sequence, it does not belong to *Homo sapiens*. In spite of this shortcoming, it was compared after alignment with 7BVQ. From this comparison a sequence similarity of 86% was found between the two proteins and that an Asp residue in the protein binding site plays a key role during ligand-receptor interaction. In fact, in 7JJO ISO interacts with Asp121 forming a hydrogen bond and an ionic interaction through its nitrogen group, and with Val122 by a hydrophobic interaction through the aromatic moiety, whereas in 7BVQ the crystallographic ligand carazolol interacts by two hydrogen bonds with Asp1138 (corresponding to Asp121 of 7JJO). Beside this interaction, carazolol is anchored to Asn1363 of *β*1 receptor through its hydroxyl group by an additional hydrogen bond. The binding energy value obtained after redocking of carazolol was -7.7 kcal/mol. As shown in Figure 3, in our experiments, although the four molecules might adopt different orientations in the complex, all of them accommodate in the binding site and are able to interact with the key residues of the active site, including Asp1138 (Table 1).

Table 1. Binding Energy for compounds 4, 7, 8 and 10 in the *β*1-adrenergic receptor (PDB code 7BVQ).

Compound	Binding Energy (kal/mol)
4	−8.0
7	−7.7
8	−7.5
10	−7.8
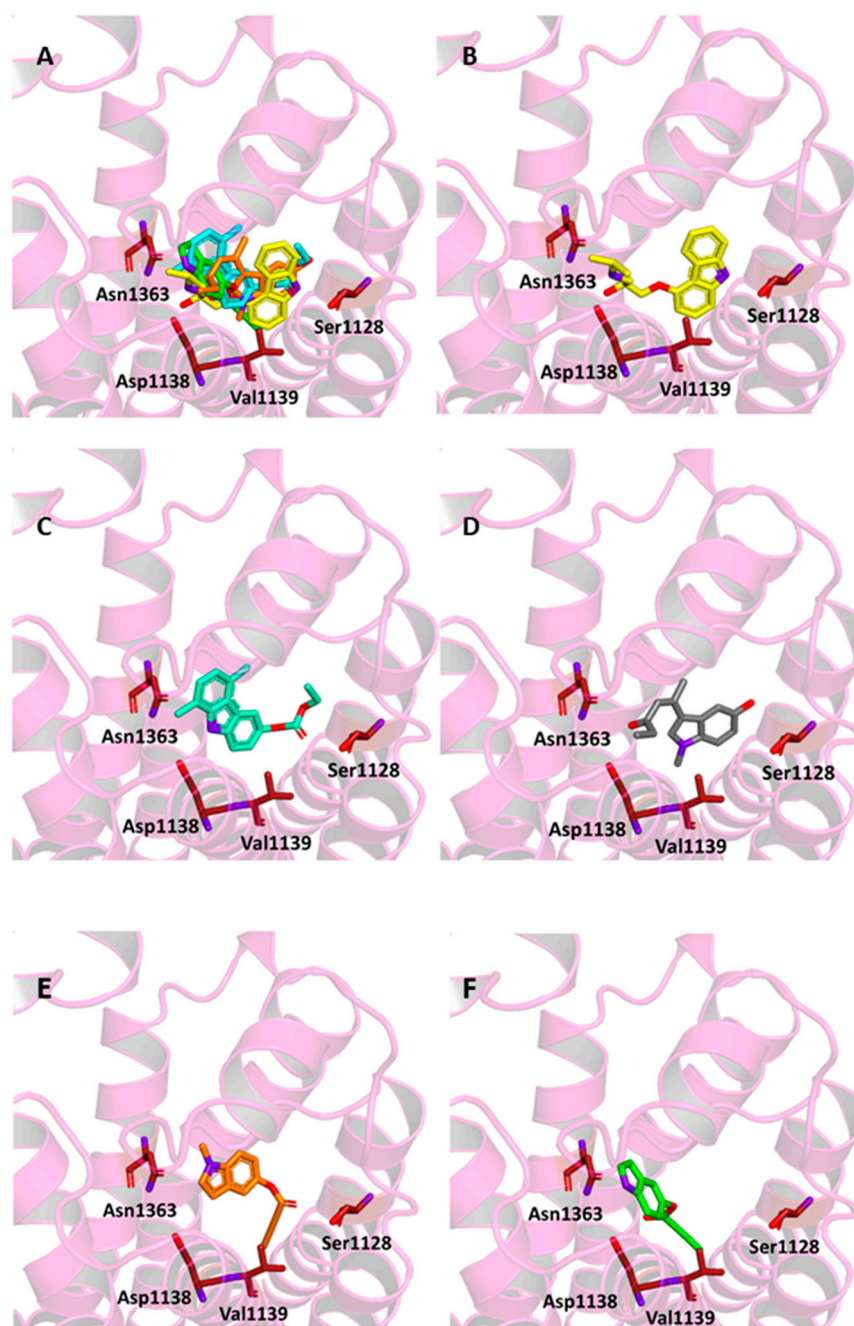
Figure 3. Ligand-binding pocket of the active site of the *β*1 adrenergic receptor. The protein backbone is represented in background as ribbons, and the key residues for ligand interaction (Asp1138, Asn1363, Ser1128, Val1139) are also indicated. (**A**) Superimposed binding modes of all the five ligands: carazolol (yellow), **4** (cyan), **7** (grey), **8** (orange) and **10** (green). Specific binding mode of carazolol (**B**), **4** (**C**), **7** (**D**), **8** (**E**) and **10** (**F**).

In particular, compound 4 interacts with the protein active site forming two hydrogen bonds: a first with Asp1138 through its carbazole nitrogen, with a distance of 3.15 Å, and the second with Ser1228 through its carbonyl group, with a distance of 2.84 Å, whereas compound 7 interacts by a hydrogen bond through its carbonyl group with Asp1138 with a distance of 3.43 Å. Compounds 8 and 10 although allocated in the same binding pocket interact through their side chain with Val1139 by hydrophobic interactions that stabilize the complexes. Overall, these results suggest that our compounds are able to accommodate in the active site of the *β*1 receptor with an affinity similar to that of the crystallographic ligands (Table 1).

3.3. In Vitro Findings

The interesting results obtained by in silico studies prompted us to investigate the biological activity exerted by compounds 4, 7, 8 and 10. Preliminary analyses indicated that compounds 4 and 7 exerted marked antiadrenergic effects on the Langendorff perfused heart model, reflecting a reduction of the cardiac performance associated with a weak cardiac recovery after washing with Krebs-Henseleit solution (unpublished data). Therefore, we aimed to deeper examine the biological activity induced by compounds 8 and 10. These molecules were tested on H9c2 cells alone or in the presence of ISO, widely used as inducer of myocardial stress and hypertrophy, mimicking the activation of the adrenergic and neurohumoral systems [46].

Effect of Compounds 8 and 10 on Cell Proliferation and ISO-Dependent Hypertrophy in H9c2 Cardiomyocytes

It has widely ascertained that the activation of $\beta1$- and $\beta2$-AR represents a main mechanism responsible for the progression of cardiac remodeling [47]. Although it has been shown that the expression of $\beta2$-ARs is higher compared to that of $\beta1$-ARs in both neonatal rat cardiomyocytes ($\beta1$, 36% vs. $\beta2$, 64%) [48] and in embryonic rat cardiomyocytes H9c2 cell lines [48,49], significant findings elucidated the selective contribution of $\beta1$ and $\beta2$-AR into the complex mechanisms of β-ARs-mediated adverse remodeling. Several studies also support the fact that, among the β-ARs, the $\beta1$ subtype is mainly responsible for catecholamine effects and represents the main promoter of cardiomyocyte hypertrophy, interstitial fibrosis and heart failure [50,51]. For instance, it has been reported that isoproterenol binds to $\beta1$-AR with higher affinity compared to $\beta2$-AR [52,53]. Furthermore, the isoproterenol-mediated cardiac responses were inhibited by betaxolol, a $\beta1$-AR antagonist, but not by ICI 118551, a $\beta2$-AR antagonist. These effects were observed both in vitro (i.e., primary cultures of cardiac ventricular myocytes stimulated with isoproterenol) and in vivo (i.e., rats exposed to continuous infusion of isoproterenol) [48]. Overall, these observations strongly suggest that the $\beta1$-subtype predominantly mediates isoproterenol-dependent hypertrophy in the heart.

Accordingly, to assess the effects of compounds 8 and 10 on cell viability, we first exposed H9c2 cells to increasing concentrations (1 to 100 nM) of each compound and their cytotoxic potential was evaluated by MTT assay. As shown in Figure 4A, compound 8 did not exert significant effects on cell proliferation at any tested concentration compared to the control cells, while compound 10 induced a significant increase in cardiac cell viability at 10 nM and 50 nM (Figure 4B). These data indicate that both compounds do not negatively affect cell viability and do not show direct cytotoxic effects.

Taking into consideration these results, we evaluated the in vitro effects of compounds 8 and 10 against cardiomyocytes hypertrophy. Therefore, we exposed H9c2 cells to ISO at 100 μM for 24 h [36], in the presence or absence of compound 8 or compound 10. Morphological staining analysis revealed that ISO treatment induced a significant increase in cardiac cell size with respect to control cells, indicating that the model of in vitro hypertrophy was successfully established (Figure 5A). Notably, compound 8 resulted was effective in significantly reducing cell size compared to the ISO group only at concentrations of 25 nM and 100 nM. Cells treated with compound 8 alone did not show significant increase in cell size (Figure 5A). The surface area analysis of H9c2 cells reflected the same trend (Figure 5B).
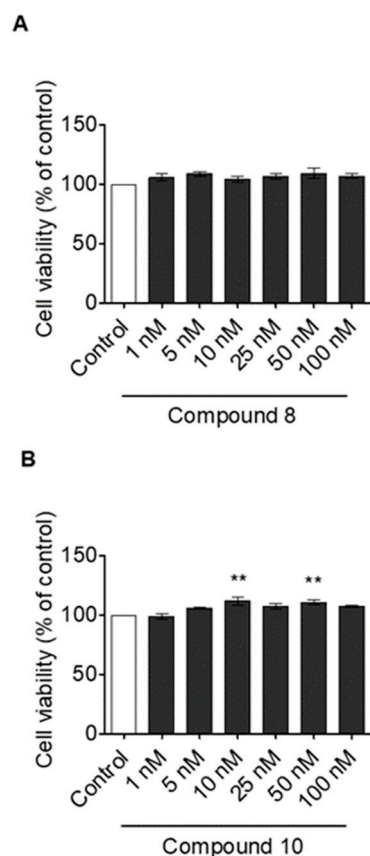
Figure 4. Effects of compounds 8 and 10 on cell viability in H9c2 cardiomyocytes. H9c2 cells were treated with vehicle (Control) or increasing concentrations of (**A**) compound **8** (1 nM–100 nM) or (**B**) compound **10** (1 nM–100 nM) for 24 h. Cell viability was determined using the MTT assay and was expressed as the percentage of control cells exposed only to vehicle (indicated as Control). Results are represented as mean $\pm$ SEM (n = 6 per group). Significant differences were detected by one-way ANOVA followed by Dunnett's test, $p < 0.01$ (**) vs. Control group.

The same experiment was carried out for testing the activity of compound 10. In this case, as evinced by morphological staining and cell surface area analysis shown in Figure 6, ISO-treated cells exhibited a significant cardiac cell size increase compared to the control cells. Conversely, in the ISO + compound 10 (10 nM) treated group, cell size was significantly decreased compared to those treated with ISO alone. Compound 10 was unable to counteract in a significant manner the effects of ISO at higher doses (25 to 100 nM). These findings indicate that, similar to compound 8, compound 10 was able to counteract ISO-dependent effects on H9c2 cells. However, the first effective dose of compound 10 was lower than that of compound 8 (10 nM vs. 25 nM). Figure 6 also indicates that compound 10 alone did not exert significant effects on cell size at 10 nM, while this parameter was significantly increased when administered at higher doses (i.e., 50 nM and 75 nM).
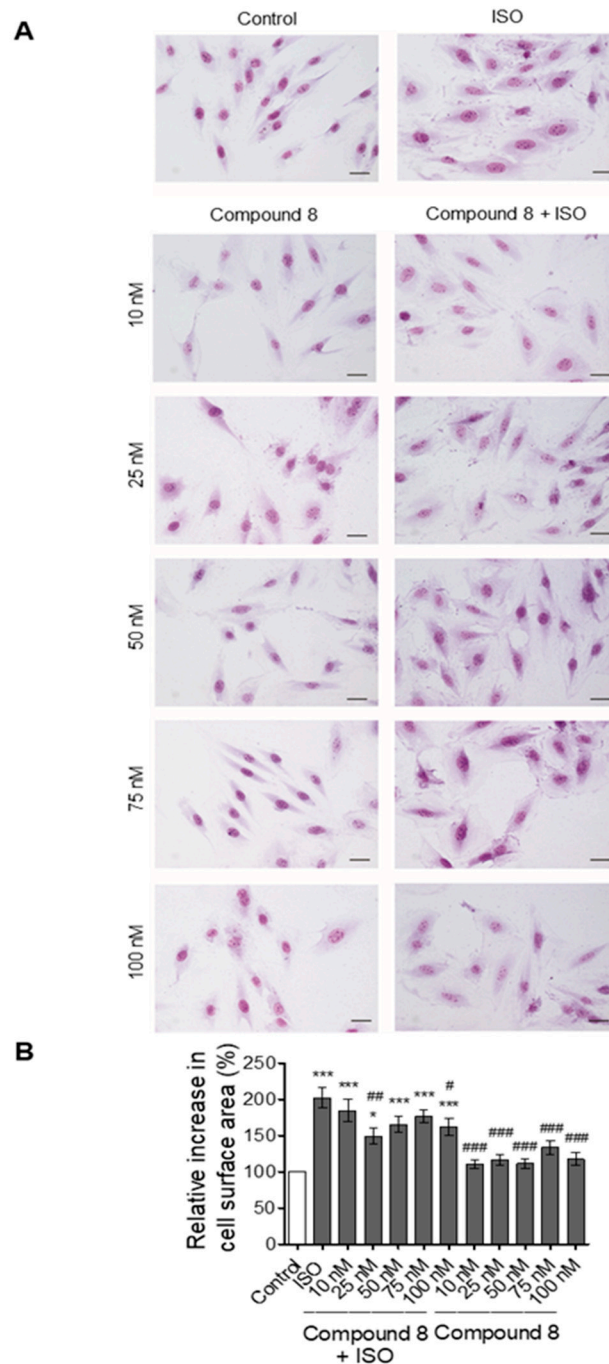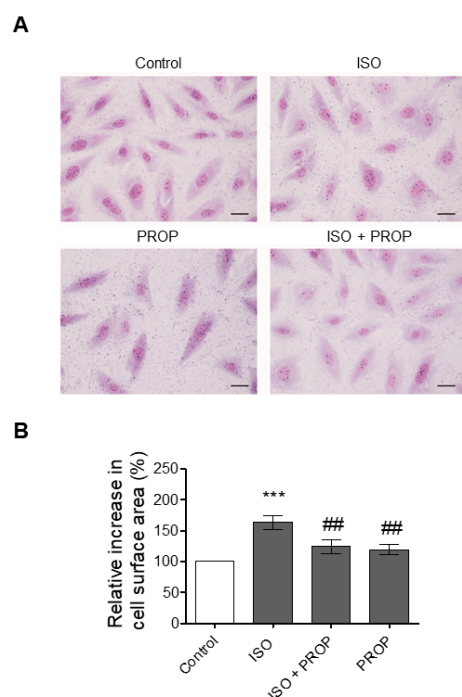
Figure 5. Effects of compound 8 on cardiomyocytes hypertrophy induced by isoproterenol (ISO) in vitro. (**A**) Morphological staining of H9c2 cells exposed to vehicle (indicated as Control), ISO (100 μM), ISO + compound 8 (from 10 nM to 100 nM) and compound **8** (from 10 nM to 100 nM) for 24 h. Scale bars: 25 μm. (**B**) Cell surface area (%) of H9c2 cells exposed to vehicle (indicated as Control), ISO (100 μM), ISO + compound 8 (from 10 nM to 100 nM) and compound 8 (from 10 nM to 100 nM) for 24 h. Data are expressed as mean $\pm$ SEM derived from two independent measurements for each group. $p < 0.05$ (*); $p < 0.001$ (***) vs. Control group; $p < 0.05$ (#); $p < 0.01$ (##); $p < 0.001$ (###) vs. ISO group (one-way ANOVA and Newman-Keuls multiple comparison test).
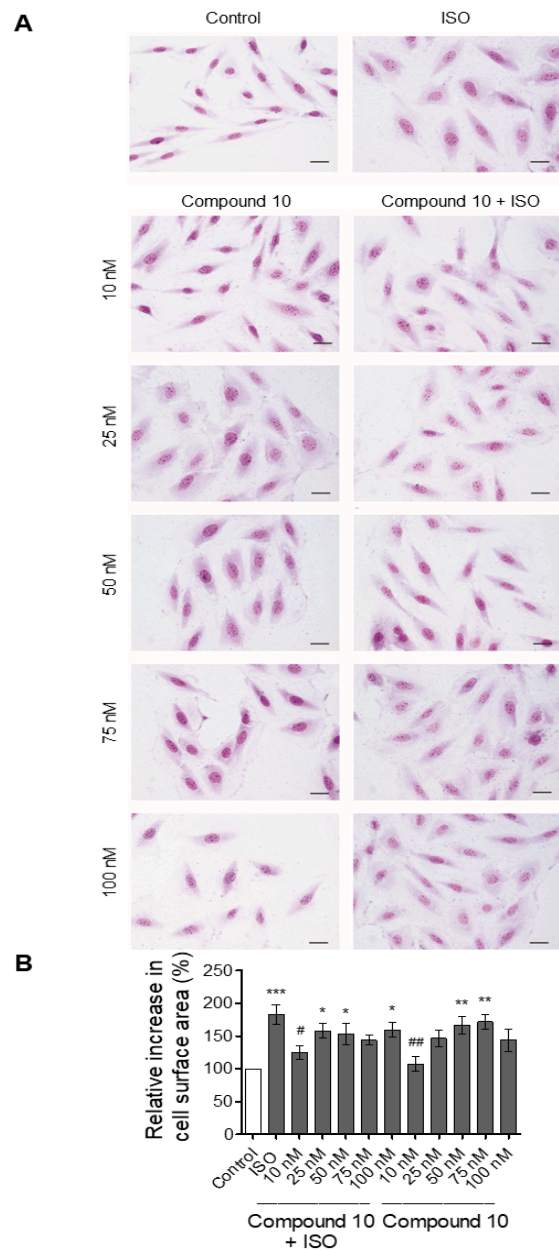
Figure 6. Effects of compound 10 on cardiomyocytes hypertrophy induced by isoproterenol (ISO) in vitro. (**A**) Morphological staining of H9c2 cells exposed to vehicle (indicated as Control), ISO (100 μM), ISO + compound 10 (from 10 nM to 100 nM) and compound 10 (from 10 nM to 100 nM) for 24 h. Scale bars: 25 μm. (**B**) Cell surface area (%) of H9c2 cells exposed to vehicle (indicated as Control), ISO (100 μM), ISO + compound 10 (from 10 nM to 100 nM) and compound 10 (from 10 nM to 100 nM) for 24 h. Data are expressed as mean $\pm$ SEM derived from two independent measurements for each group. $p < 0.05$ (*); $p < 0.01$ (**); $p < 0.001$ (***) vs. Control group; $p < 0.05$ (#); $p < 0.01$ (##) vs. ISO group (one-way ANOVA and Newman-Keuls multiple comparison test).

Our data are of interest in the view of β-blocker monitoring and dosing, to avoid or minimize their side effects [54]. β-blockers reach their therapeutic goal mainly by inducing negative chronotropic effects that prolong heart diastole and rest. In this context the choice of an appropriate dose is vital to avoid concomitant adverse negative inotropic effects.

Accordingly, we used the β-adrenergic receptor antagonist propranolol as a positive control. As depicted in Figure 7, both morphological staining and cell surface area indicated that in H9c2 cotreated with propranolol (1 μM), ISO failed to increase cardiomyocyte size.

Figure 7. Effects of propranolol (PROP) on cardiomyocytes hypertrophy induced by isoproterenol (ISO) in vitro. (**A**) Morphological staining of H9c2 cells exposed to vehicle (indicated as Control), ISO (100 μM), ISO + propranolol (PROP) (1 μM) and propranolol (1 μM) for 24 h. Scale bars: 25 μm. (**B**) Cell surface area (%) of H9c2 cells exposed to vehicle (indicated as Control), ISO (100 μM), ISO + propranolol (PROP) (1 μM) and propranolol (1 μM) for 24 h. Data are expressed as mean ± SEM derived from two independent measurements for each group. $p < 0.001$ (***) vs. Control group; $p < 0.01$ (##) vs. ISO group (one-way ANOVA and Newman-Keuls multiple comparison test).

Our compounds were effective at lower doses (nM range) with respect to the classic β-blocker propranolol (μM range), according to data that support beneficial effects of low dosage especially in patients suffering from ventricular hypertrophy [55]. Clinical evidence indicates that, in practice, β-blockers are often used at half or lower doses compared to manufacturers' recommendations [56]. For some drugs, lower doses even improved the disease outcomes [57]. In the specific case of β-blockers, much data indicate their best use at the lowest effective dose [58].

4. Conclusions

In summary, our in silico results support the hypothesis that compounds 4, 7, 8 and 10 could interact with the active binding site of β1-AR. Moreover, compounds 8 and 10 emerged as potential counteracting agents against ISO-dependent in vitro cardiac hypertrophy. These data are of additional interest considering that the effect of the two molecules was achieved starting from lower concentrations compared to those of the traditional β-AR antagonist propranolol. In this context, our compounds could act as more potent pharmacological agents (i.e., β1-blockers), and their lower effective doses may contribute to minimize their adverse effects. Altogether, our findings depict the studied molecules worthy of further in vivo investigation.

Author Contributions: Conceptualization, A.C. (Anna Caruso) and T.A.; methodology, F.G., A.D.B.; validation, A.C. (Alessia Carocci), T.A.; formal analysis, V.R. and M.A.O.; investigation, T.P. and M.A.O.; writing—original draft preparation, F.G., A.C. (Anna Caruso) and C.R. writing—review and editing, A.C. (Anna Caruso) and M.S.S.; supervision, M.S.S. All authors have read and agreed to the published version of the manuscript.

References

1. Do Vale, G.T.; Ceron, C.S.; Gonzaga, N.A.; Simplicio, J.A.; Padovan, J.C. Three generations of β-blockers: History, class differences and clinical applicability. *Curr. Hypertens. Rev.* **2018**, *15*, 22–31. [CrossRef] [PubMed]
2. Oliver, E.; Mayor, F., Jr.; D'Ocon, P. Beta-blockers: Historical Perspective and mechanisms of action. *Rev. Española Cardiol.* **2019**, *72*, 853–862. [CrossRef]
3. Dale, H.H. On some physiological actions of ergot. *J. Physiol.* **1906**, *34*, 163–206. [CrossRef]
4. Wang, J.; Gareri, C.; Rockman, H.A. G-protein-coupled receptors in heart disease. *Circ. Res.* **2018**, *123*, 716–735. [CrossRef]
5. Moran, N.C.; Perkins, M.E. Adrenergic blockade of the mammalian heart by a dichloro analogue of isoproterenol. *J. Pharm. Exp. Ther.* **1958**, *124*, 223–237.
6. Quirke, V. Putting theory into practice: James Black, receptor theory and the development of the beta-blockers at ICI, 1958–1978. *Med. Hist.* **2006**, *50*, 69–92. [CrossRef] [PubMed]
7. Pfleger, J.; Gresham, K.; Koch, W.J. G protein-coupled receptor kinases as therapeutic targets in the heart. *Nat. Rev. Cardiol.* **2019**, *16*, 612–622. [CrossRef]
8. Giltrow, E.; Eccles, P.D.; Hutchinson, T.H.; Sumpter, J.P.; Rand-Weaver, M. Characterisation and expression of β1-, β2- and β3-adrenergic receptors in the fathead minnow (*Pimephales promelas*). *Gen. Comp. Endocrinol.* **2011**, *173*, 483–490. [CrossRef]
9. Leo, S.; Gattuso, A.; Mazza, R.; Filice, M.; Cerra, M.C.; Imbrogno, S. Cardiac influence of the β3-adrenoceptor in the goldfish (*Carassius auratus*): A protective role under hypoxia? *J. Exp. Biol.* **2019**, *222*, jeb211334. [CrossRef]
10. Imbrogno, S.; Filice, M.; Cerra, M.C. Exploring cardiac plasticity in teleost: The role of humoral modulation. *Gen. Comp. Endocrinol.* **2019**, *283*, 113236. [CrossRef]
11. De Lucia, C.; Eguchi, A.; Koch, W.J. New insights in cardiac β-Adrenergic signaling during heart failure and aging. *Front. Pharm.* **2018**, *9*, 904. [CrossRef]
12. Baker, J.G.; Hill, S.J.; Summers, R.J. Evolution of β-blockers: From anti-anginal drugs to ligand-directed signalling. *Trends Pharm. Sci.* **2011**, *32*, 227–234. [CrossRef]
13. Poirier, L.; Tobe, S.W. Contemporary use of β-blockers: Clinical relevance of subclassification. *Can. J. Cardiol.* **2014**, *30*, S9–S15. [CrossRef] [PubMed]
14. Han, J.W.; Kang, C.; Kim, Y.; Lee, M.G.; Kim, J.Y. Isoproterenol-induced hypertrophy of neonatal cardiac myocytes and H9c2 cell is dependent on TRPC3-regulated CaV1.2 expression. *Cell Calcium* **2020**, *92*, 102305. [CrossRef]
15. Hescheler, J.; Meyer, R.; Plant, S.; Krautwurst, D.; Rosenthal, W.; Schultz, G. Morphological, biochemical, and electrophysiological characterization of a clonal cell (H9c2) line from rat heart. *Circ. Res.* **1991**, *69*, 1476–1486. [CrossRef]
16. Angelone, T.; Caruso, A.; Rochais, C.; Caputo, A.M.; Cerra, M.C.; Dallemagne, P.; Filice, E.; Genest, D.; Pasqua, T.; Puoci, F.; et al. Indenopyrazole oxime ethers: Synthesis and β1-adrenergic blocking activity. *Eur. J. Med. Chem.* **2015**, *92*, 672–681. [CrossRef]
17. Grande, F.; Parisi, O.I.; Mordocco, R.A.; Rocca, C.; Puoci, F.; Scrivano, L.; Quintieri, A.M.; Cantafio, P.; Ferla, S.; Brancale, A.; et al. Quercetin derivatives as novel antihypertensive agents: Synthesis and physiological characterization. *Eur. J. Pharm. Sci.* **2016**, *82*, 161–170. [CrossRef] [PubMed]
18. Di Nunno, L.; Franchini, C.; Scilimati, A.; Sinicropi, M.S.; Tortorella, P. Chemical and chemoenzymatic routes to 1-(benzothiazol-2-ylsulfanyl)-3-chloropropan-2-ol, a precursor of drugs with potential β-blocker activity. *Tetrahedron Asymmetry* **2000**, *11*, 1571–1583. [CrossRef]
19. Go, J.G.; Santiago, L.D.; Miranda, A.C.; Jara, R.D. Effect of Beta-blockers on Hypertension and Heart Failure with Reduced Ejection Fraction: A Systematic Review of Randomized Controlled Trials. *Hypertens. J.* **2019**, *5*. [CrossRef]
20. Bennett, M.; Chang, C.L.; Tatley, M.; Savage, R.; Hancox, R.J. The safety of cardio-selective beta1-blockers in asthma: Literature review and search of global pharmacovigilance safety reports. *ERJ Open Res.* **2021**, *7*, 00801–02020. [CrossRef] [PubMed]
21. Chang, A.; Yeung, S.; Thakkar, A.; Huang, K.M.; Liu, M.M.; Kanassatega, R.-S.; Parsa, C.; Orlando, R.; Jackson, E.K.; Andresen, B.T.; et al. Prevention of skin carcinogenesis by the β-blocker carvedilol. *Prev. Cancer Prev. Res.* **2015**, *8*, 27–36. [CrossRef] [PubMed]
22. Xu, X.; Kaindl, J.; Clark, M.J.; Hübner, H.; Hirata, K.; Sunahara, R.K.; Gmeiner, P.; Kobilka, B.K.; Liu, X. Binding pathway determines norepinephrine selectivity for the human β1AR over β2AR. *Cell Res.* **2021**, *31*, 569–579. [CrossRef]

23. Wong, G.W.K.; Boyda, H.N.; Wright, J.M. Blood pressure lowering efficacy of partial agonist beta blocker monotherapy for primary hypertension. *Cochrane Database Syst. Rev.* **2014**, *12*, 2017. [CrossRef]

24. Willette, R.N.; Mitchell, M.P.; Ohlstein, E.H.; Lukas, M.A.; Ruffolo, R.R. Evaluation of intrinsic sympathomimetic activity of bucindolol and carvedilol in rat heart. *Pharmacology* **1998**, *56*, 30–36. [CrossRef] [PubMed]

25. Caruso, A.; Sophie Voisin-Chiret, A.; Lancelot, J.-C.; Sinicropi, S.; Garofalo, A.; Rault, S. Novel and efficient synthesis of 5,8-dimethyl-9h-carbazol-3-ol via a hydroxydeboronation reaction. *Heterocycles* **2007**, *71*, 2203–2210. [CrossRef]

26. Saturnino, C.; Grande, F.; Aquaro, S.; Caruso, A.; Iacopetta, D.; Bonomo, M.; Longo, P.; Schols, D.; Sinicropi, M. Chloro-1,4-dimethyl-9H-carbazole Derivatives Displaying Anti-HIV Activity. *Molecules* **2018**, *23*, 286. [CrossRef] [PubMed]

27. Rizza, P.; Pellegrino, M.; Caruso, A.; Iacopetta, D.; Sinicropi, M.S.; Rault, S.; Lancelot, J.C.; El-Kashef, H.; Lesnard, A.; Rochais, C.; et al. 3-(Dipropylamino)-5-hydroxybenzofuro[2,3-*f*]quinazolin-1(2*H*)-one (DPA-HBFQ-1) plays an inhibitory role on breast cancer cell growth and progression. *Eur. J. Med. Chem.* **2016**, *107*, 275–287. [CrossRef]

28. Sinicropi, M.S.; Iacopetta, D.; Rosano, C.; Randino, R.; Caruso, A.; Saturnino, C.; Muià, N.; Ceramella, J.; Puoci, F.; Rodriquez, M.; et al. *N*-thioalkylcarbazoles derivatives as new anti-proliferative agents: Synthesis, characterisation and molecular mechanism evaluation. *J. Enzym. Inhib. Med. Chem.* **2018**, *33*, 434–444. [CrossRef]

29. Caruso, A.; Lancelot, J.C.; El-Kashef, H.; Sinicropi, M.S.; Legay, R.; Lesnard, A.; Rault, S. A rapid and versatile synthesis of novel pyrimido[5,4-b]carbazoles. *Tetrahedron* **2009**, *65*, 10400–10405. [CrossRef]

30. Saturnino, C.; Caruso, A.; Longo, P.; Capasso, A.; Pingitore, A.; Caroleo, M.; Cione, E.; Perri, M.; Nicolo, F.; Nardo, V.; et al. Crystallographic Study and Biological Evaluation of 1,4-dimethyl-*N*-alkylcarbazoles. *Curr. Top. Med. Chem.* **2015**, *15*, 973–979. [CrossRef]

31. Hanwell, M.D.; Curtis, D.E.; Lonie, D.C.; Vandermeerschd, T.; Zurek, E.; Hutchison, G.R. Avogadro: An advanced semantic chemical editor, visualization, and analysis platform. *J. Cheminform.* **2012**, *4*, 17. [CrossRef]

32. Morris, G.M.; Goodsell, D.S.; Halliday, R.S.; Huey, R.; Hart, W.E.; Belew, R.K.; Olson, A.J. Automated docking using a Lamarckian genetic algorithm and an empirical binding free energy function. *J. Comput. Chem.* **1998**, *19*, 1639–1662. [CrossRef]

33. Trott, O.; Olson, A.J. AutoDock Vina: Improving the speed and accuracy of docking with a new scoring function, efficient optimization, and multithreading. *J. Comput. Chem.* **2010**, *31*, 455–461. [CrossRef]

34. Grande, F.; Rizzuti, B.; Occhiuzzi, M.A.; Ioele, G.; Casacchia, T.; Gelmini, F.; Guzzi, R.; Garofalo, A.; Statti, G. Identification by molecular docking of homoisoflavones from leopoldia comosa as ligands of estrogen receptors. *Molecules* **2018**, *23*, 894. [CrossRef]

35. Casacchia, T.; Occhiuzzi, M.A.; Grande, F.; Rizzuti, B.; Granieri, M.C.; Rocca, C.; Gattuso, A.; Garofalo, A.; Angelone, T.; Statti, G. A pilot study on the nutraceutical properties of the Citrus hybrid Tacle® as a dietary source of polyphenols for supplementation in metabolic disorders. *J. Funct. Foods* **2019**, *52*, 370–381. [CrossRef]

36. Rocca, C.; Grande, F.; Granieri, M.C.; Colombo, B.; De Bartolo, A.; Giordano, F.; Rago, V.; Amodio, N.; Tota, B.; Cerra, M.C.; et al. The chromogranin A$_{1-373}$ fragment reveals how a single change in the protein sequence exerts strong cardioregulatory effects by engaging neuropilin-1. *Acta Physiol.* **2020**, *231*, e13570.

37. Rocca, C.; Femminò, S.; Aquila, G.; Granieri, M.C.; De Francesco, E.M.; Pasqua, T.; Rigiracciolo, D.C.; Fortini, F.; Cerra, M.C.; Maggiolini, M.; et al. Notch1 mediates preconditioning protection induced by gper in normotensive and hypertensive female rat hearts. *Front. Physiol.* **2018**, *9*, 521. [CrossRef]

38. Nettore, I.C.; Rocca, C.; Mancino, G.; Albano, L.; Amelio, D.; Grande, F.; Puoci, F.; Pasqua, T.; Desiderio, S.; Mazza, R.; et al. Quercetin and its derivative Q2 modulate chromatin dynamics in adipogenesis and Q2 prevents obesity and metabolic disorders in rats. *J. Nutr. Biochem.* **2019**, *69*, 151–162. [CrossRef]

39. Rocca, C.; De Bartolo, A.; Grande, F.; Rizzuti, B.; Pasqua, T.; Giordano, F.; Granieri, M.C.; Occhiuzzi, M.A.; Garofalo, A.; Amodio, N.; et al. Cateslytin abrogates lipopolysaccharide-induced cardiomyocyte injury by reducing inflammation and oxidative stress through toll like receptor 4 interaction. *Int. Immunopharmacol.* **2021**, *94*, 107487. [CrossRef]

40. Cai, L.; Fan, G.; Wang, F.; Liu, S.; Li, T.; Cong, X.; Chun, J.; Chen, X. Protective role for LPA3 in cardiac hypertrophy induced by myocardial infarction but not by isoproterenol. *Front. Physiol.* **2017**, *8*, 356. [CrossRef]

41. Sinicropi, M.S.; Caruso, A.; Conforti, F.; Marrelli, M.; El Kashef, H.; Lancelot, J.; Rault, S.; Statti, G.A.; Menichini, F. Synthesis, inhibition of NO production and antiproliferative activities of some indole derivatives. *J. Enzyme Inhib. Med. Chem.* **2009**, *24*, 1148–1153. [CrossRef]

42. Cranwell, P.A.; Saxton, J.E. A synthesis of ellipticine. *J. Chem. Soc.* **1962**, *683*, 3482–3487. [CrossRef]

43. Letois, B.; Lancelot, J.; Rault, S.; Robba, M.; Tabka, T.; Gauduchon, P.; Bertreux, E.; Le Talaer, J. Étude de la cytotoxicitéin vitro de dérivés du carbazole III. 3-Amino et 3-nitro-1,4-diméthyl-9H-carbazoles diversement substitués en position. *Eur. J. Med. Chem.* **1990**, *25*, 775–784.

44. Yadav, M.R.; Grande, F.; Chouhan, B.S.; Naik, P.P.; Giridhar, R.; Garofalo, A.; Neamati, N. Cytotoxic potential of novel 6,7-dimethoxyquinazolines. *Eur. J. Med. Chem.* **2012**, *48*, 231–243. [CrossRef] [PubMed]

45. Caruso, A.; Chimento, A.; El-Kashef, H.; Lancelot, J.-C.; Panno, A.; Pezzi, V.; Saturnino, C.; Sinicropi, M.S.; Sirianni, R.; Rault, S. Antiproliferative activity of some 1,4-dimethylcarbazoles on cells that express estrogen receptors: Part I. *J. Enzyme Inhib. Med. Chem.* **2012**, *27*, 609–613. [CrossRef]

46. Lymperopoulos, A.; Rengo, G.; Koch, W.J. Adrenergic nervous system in heart failure: Pathophysiology and therapy. *Circ. Res.* **2013**, *113*, 739–753. [CrossRef] [PubMed]

47. Xu, Q.; Dalic, A.; Fang, L.; Kiriazis, H.; Ritchie, R.H.; Sim, K.; Gao, X.M.; Drummond, G.; Sarwar, M.; Zhang, Y.Y.; et al. Myocardial oxidative stress contributes to transgenic β 2- adrenoceptor activation-induced cardiomyopathy and heart failure. *Br. J. Pharm.* **2011**, *162*, 1012–1028. [CrossRef]

48. Morisco, C.; Zebrowski, D.C.; Vatner, D.E.; Vatner, S.F.; Sadoshima, J. β-adrenergic cardiac hypertrophy is mediated primarily by the β$_1$-subtype in the rat heart. *J. Mol. Cell. Cardiol.* **2001**, *33*, 561–573. [CrossRef]

49. Dangel, V.; Giray, J.; Ratge, D.; Wisser, H. Regulation of β-adrenoceptor density and mRNA levels in the rat heart cell-line H9c. *Biochem. J.* **1996**, *317*, 925–931. [CrossRef]

50. Lohse, M.J.; Engelhardt, S.; Eschenhagen, T. What is the role of β-adrenergic signaling in heart failure? *Circ. Res.* **2003**, *93*, 896–906. [CrossRef]

51. Vidal, M.; Wieland, T.; Lohse, M.J.; Lorenz, K. β-Adrenergic receptor stimulation causes cardiac hypertrophy via a Gβγ/Erk-dependent pathway. *Cardiovasc. Res.* **2012**, *96*, 255–264. [CrossRef]

52. Hoffmann, C.; Leitz, M.R.; Oberdorf-Maass, S.; Lohse, M.J.; Klotz, K.N. Comparative pharmacology of human β-adrenergic receptor subtypes-characterization of stably transfected receptors in CHO cells. *Naunyn. Schmiedebergs. Arch. Pharm.* **2004**, *369*, 151–159. [CrossRef] [PubMed]

53. Del Carmine, R.; Ambrosio, C.; Sbraccia, M.; Cotecchia, S.; Ijzerman, A.P.; Costa, T. Mutations inducing divergent shifts of constitutive activity reveal different modes of binding among catecholamine analogues to the β$_2$-adrenergic receptor. *Br. J. Pharm.* **2002**, *135*, 1715–1722. [CrossRef] [PubMed]

54. Basile, J.N. Titration of β-blockers in heart failure: How to maximize benefit while minimizing adverse events. *Postgrad Med.* **2003**, *113*, 63–70. [CrossRef]

55. Schmitt, B.; Li, T.; Kutty, S.; Khasheei, A.; Schmitt, K.R.L.; Anderson, R.H.; Lunkenheimer, P.P.; Berger, F.; Kühne, T.; Peters, B. Call for papers impact of sympathoexcitation on cardiovascular function in humans effects of incremental beta-blocker dosing on myocardial mechanics of the human left ventricle: MRI 3D-tagging insight into pharmacodynamics supports theory of inner antagonism. *Am. J. Physiol. Heart Circ. Physiol.* **2015**, *309*, H45–H52.

56. Gislason, G.H.; Rasmussen, J.N.; Abildstrøm, S.Z.; Gadsbøll, N.; Buch, P.; Friberg, J.; Rasmussen, S.; Køber, L.; Stender, S.; Madsen, M.; et al. Long-term compliance with beta-blockers, angiotensin-converting enzyme inhibitors, and statins after acute myocardial infarction. *Eur. Heart J.* **2006**, *27*, 1153–1158. [CrossRef] [PubMed]

57. Dimmitt, S.B.; Stampfer, H.G. Low drug doses may improve outcomes in chronic disease. *Med. J. Aust.* **2009**, *191*, 511–513. [CrossRef] [PubMed]

58. Dimmitt, S.B.; Stampfer, H.G.; Warren, J.B. β-adrenoceptor blockers valuable but higher doses not necessary. *Br. J. Clin. Pharm.* **2014**, *78*, 1076–1079. [CrossRef]